NATURE OF STRAIN HARDENING IN POLYCRYSTALLINE INDIAN COMMERCIAL ALUMINUM

By Y. V. R. K. PRASAD, D. H. SASTRY AND K. I. VASU

Materials Research Group, Department of Metallurgy, Indian Institute of Science, Bangalore 12, India

[Received: March 1, 1969]

ABSTRACT

A description of the constant-stress-creep testing unit and constant strain-rate tensile testing machine, designed and built in the Department is given. The nature of strain hardening in Indian commercial aluminum is investigated with the help of combined data on creep tests at 86°K and tensile tests in the temperature range 86° – 473°K at two strain rates. The engineering tensile deformation data are also presented. The activation volume (2×10^{-21} cm^3) and total activation energy (0·75 eV) for the rate-controlling dislocation mechanism are estimated. The thermally activated non-conservative motion of jogs leading to point defect production is discussed in the light of the present data.

1. INTRODUCTION

Because of its abundance, aluminum in India finds a wide variety of engineering applications. Depending upon the requirement, the strength of this metal is improved by alloying, heat treatment and cold working. For applications like air-craft industry, alloying and heat-treatment yield the required specification of high strength-to-weight ratio. Cold working might also provide a cheap and potential method of improving the strength property of aluminum. As a result of cold work, the metal gets strain hardened, the amount of hardening being more, the lower the temperature of working. No systematic study has yet been made on the nature of strain hardening in Indian commercial aluminum except that it was shown[1] to exhibit logarithmic creep even at room temperature in contrast to high purity aluminum which shows recovery creep[2] above 200°K. This was thought to be due to the effect of impurities present in the commercial metal.

Strain hardening in metals has been studied extensively. Theories based on highly idealized dislocation models have been developed[3–5]. Models based on continuum mechanics approach have also been proposed[6] to explain strain hardening. It can be said that strain hardening occurs as a result of interaction between dislocations on primary and secondary slip systems, which provides

effective obstacles for further dislocation movement. The nature of the obstacles to dislocation motion decides the extent of hardening that can be achieved by cold work.

Many investigations have been conducted[7-11] to understand the nature of obstacles to dislocation motion and to evaluate the rate-controlling dislocation mechanism in aluminum. These indicate that in high purity aluminum[9-11], below about 200°K, the "forest" dislocations act as effective obstacles and the intersection of glide and forest dislocations may be the rate-controlling mechanism. Although the presence of impurities appears to affect the nature of deformation, their exact influence on the mechanism is not understood.

The aim of the present investigation is to obtain engineering data on the strength property of Indian aluminum at different temperatures and to examine the nature of deformation at low temperatures in the light of the above mentioned information.

2. THEORY OF THERMALLY ACTIVATED DEFORMATION

Initial flow stress. It is now generally established that the low temperature plastic flow in *f. c. c.* metals occurs by thermally activated processes[12] enabling one to separate the flow stress τ for a given strain hardened state into two components :

$$\tau = \tau^* + \tau_G \qquad [1]$$

where τ_G is the stress required to overcome the long range barriers to dislocation motion and τ^* is the temperature and strain-rate dependent stress controlled by short range obstacles. Thermal fluctuations can assist the applied stress in overcoming the short range barriers since the energy required is only small.

Several forces may contribute to flow stress and it is difficult to evaluate the rate-controlling mechanism or to evaluate the relative contributions from different forces. The possible processes determining the yield stress are Peierls-Nabarro force (which is not significant in "soft" group metals), intersection of dislocations, piled-up group of dislocations and non-conservative motion of jogs. As piled-up groups of dislocations are not usually observed in high stacking fault-energy metals like aluminum, the most probable ones are either intersection of dislocations or the non-conservative motion of jogs. The theory suggestd by Seeger[12] based on the intersection mechanism is realised to be only an approximation because the exact nature of the barrier is not reasonably known.

Temperature and strain rate effects. Seeger[12] suggested that the rate of flow of *f.c.c.* metals at low temperatures is controlled by thermally activated intersection mechanism as given by :

$$\dot{\varepsilon} = NAb\nu \exp(-U/kT) \qquad [2]$$

where $\dot{\epsilon}$ = strain rate, N = number of dislocation elements per unit volume that is participating in the activation event, A = area swept out per successful intersection, b = Burgers vector, ν = vibrational frequency of the dislocation, U = activation energy that must be supplied by thermal fluctuations to the applied stress for the completion of the thermally activated process, k = Boltzmann constant and T = the absolute temperature.

Because, for intersection, a successful thermal fluctuation must complete the constriction and form a jog, Basinski[8] pointed out,

$$U = \int_{F=(\tau-\tau_G)\,L,b}^{F_m} x\,dF \qquad [3]$$

where $F-x$ curve gives the force-displacement diagram for intersection at the test temperature, F_m being the maximum force required to complete intersection. L gives the average spacing between forest dislocations. Whereas Hirsch[13] and Basinski[8], in view of the constancy of Cottrell-Stokes ratio[14] with strain, have suggested that τ_G arises only from the local stress fields at the point of intersection, Dorn and coworkers[9, 11] have shown that τ_G is a combination of stresses due to local interactions of the glide and forest dislocations and from long range stress fields. The origin of the long range stress fields may be due to piled-up groups of dislocations or elastic interactions in the tangled dislocations.

The nature of $F-x$ profile was determined by Basinski[8] and Dorn and coworkers[9, 11] from data on the change of flow stress associated with a change in strain rate during constant-temperature tensile tests. The method adopted by the latter authors is to obtain a flow parameter B, defined as

$$B = \frac{\Delta \ln \dot{\epsilon}}{\Delta T} \simeq \frac{\partial \ln \dot{\epsilon}}{\partial T} = \frac{x.L.b}{kT} \qquad [4]$$

as a function of stress. By assuming $b \simeq x$ at $4°K$, it was possible to arrive at the values of forest spacing, L, as a function of stress and temperature. The change in L with stress was then eliminated from the stress dependence of B to arrive at the variation of x with force.

A simplifying assumption, which helps to bring out in a lucid way the influence of various factors, is to suppose that the activation energy is a linear function of applied stress in such a way that one can take a square topped curve for F-x variation. If the variation as suggested by the experiment is considered instead of a square-topped curve, the effect is to reduce the activation distance and total activation energy with stress and the energy required for thermal activation decreases more rapidly with increase in stress than for a square-topped curve. The distance through which the stress moves the dislocation line during thermal activation also decreases.

In spite of the above approximations, for mathematical simplicity, the following arguments are based on a square-topped barrier. The activation energy, $U = U_0 - (\tau - \tau_G)\, x.L.b = U_0 - \tau^* v$ [5]

where v is called the " activation volume ". It is not a physical volume but is related to the area swept out in the activation event. Often, dislocation mechanisms are predicted on the basis of the " activation volume " determined from measurements of $(\partial \ln \dot{\epsilon} / \partial T)$ since from equations [2] and [5],

$$v = (\partial \ln \dot{\epsilon} / \partial T) \cdot kT \simeq (\triangle \ln \dot{\epsilon} / \triangle T) \cdot kT \simeq B k T$$

The values of B can be obtained by (*a*) measuring the change in the shear stress at the instant the strain rate is changed during a constant-strain-rate tensile test and (*b*) by measuring the change in the creep rate at the instant the applied stress is changed by $\triangle T$.

Activation energies are directly measured[15, 16] from changes in creep rate with temperature at a constant stress. But the interpretation of the results appears to be not simple because of two factors: (*a*) The number of elements getting activated changes with temperature since weaker junctions at a particular temperature become stronger at a lower temperature. These will be transparent at higher temperatures. (*b*) Error is also introduced due to the change in shear modulus with temperature.

Earlier investigations on commercially pure aluminum[17, 18] indicated that the main interaction of impurities with dislocations is the one resulting in the Cottrell-atmosphere formation. Though Suzuki locking[19] can be thought of as a possible interaction, it is doubtful whether such a small percentage of impurities (0 5%) as in commercial aluminum can widen the stacking faults to a great extent. However, the effect of impurities on the rate-controlling machanism has to be considered separately. The possibility of impurities present, as precipitates if at all, affecting the low-temperature thermally activated deformation mechanism appears to be remote[20].

3. MATERIALS AND METHODS

Indian commercial aluminum of 99 5% purity (0.05% *Cu*, 0.45% *Fe* + *Si* and traces of *Ti* and *Mg*) was melted and cast into rods, 2.5 cms. in diameter. The rods were cold rolled into sheets of about 1.25 mm. thickness maintaining the rolling direction the same throughout. Sheet specimens were punched from the sheet with the rolling direction along the guage leng.h. The specimens were then annealed at 400°C for 30 minutes and electropolished in perchloric acid-ethyl alcohol bath. The measured average grain diameter was 0.03 mm.

Tensile Testing. Tensile tests were conducted on a modified Hounsfield tensometer, a line diagram of which is shown in Fig. 1. The sheet sample,

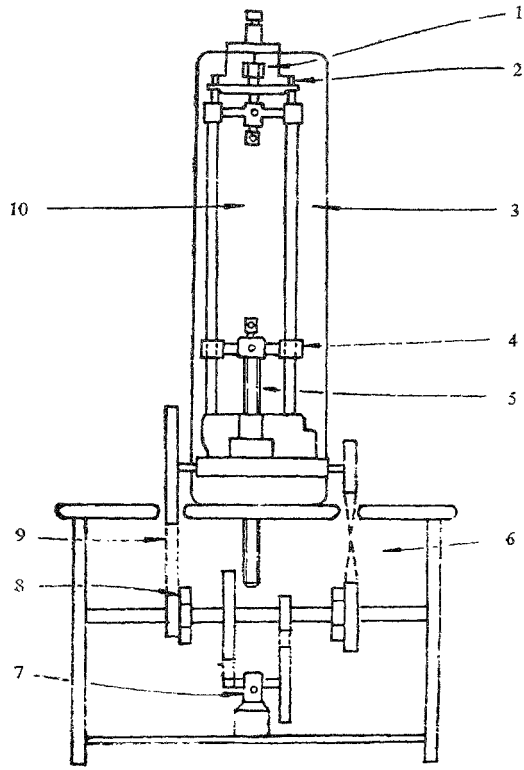

FIG. 1

Schematic line diagram of the variable speed, constant strain rate tensile testing machine:
(1) LVDT transducer (2) spring beam (3) tensometer columns (4) moving cross-head (5) drive screw (6) pulley arrangement (7) synchronous motor's reduction gear (8) free wheels (9) V-belts (10) space into which the cage shown in Fig. 2 is inserted.

fixed in a specially designed cage shown in Fig. 2, is pulled at a constant rate with the help of a pulley arrangement driven by a synchronous motor. With this arrangement, it is possible to pull the samples at rates corresponding to strain rates of 7.8×10^{-4}, 1.8×10^{-4}, 2.1×10^{-5} and 3.8×10^{-6} sec^{-1} on

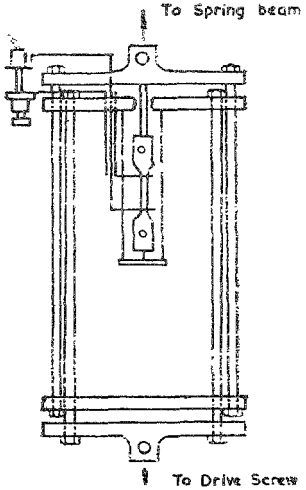

FIG. 2

Line diagram of the specimen cage used for tensile testing.

samples of 1″ gauge length. With the use of two free wheels, it is also possible to change the strain rate during the test either from 7.8×10^{-4} to 1.8×10^{-4} per second or from 2.1×10^{-5} to 3.8×10^{-6} per second and *vice versa*, by reversing the motor. The load on the sample is recorded by measuring the deflection of the 2-Ton spring beam with the help of Linear Variable Differential Transformer (LVDT) transducer, the amplified output of which is fed to a *mV* recorder. The sensitivity of the load measurement was 1.5 kg. The use of an extensometer fitted with a LVDT coil permitted recording of elongation on the gauge length continuously. The sensitivity of strain measurement was 5×10^{-4}. The specimen cage shown in Fig. 2 enabled the use of a glass Dewar as a container for the liquid used for achieving the required temperature. The testing procedure is as follows: The sample was fixed in the specimen cage and inserted in the tensometer. The cage containing the specimen is surrounded with the appropriate bath for getting the required temperature (described later). The specimen is then pulled at the required rate by choosing proper combination for the pulley arrangement. The load and extension on the sample were measured separately on two *mV* recorders.

Creep testing. Creep tests were conducted on a constant-stress-tensile creep testing unit designed and fabricated in the laboratory. The line diagram of the unit is shown in Fig. 3. The applied stress was maintained constant during the test with the help of a pre-designed smooth contour over which a steel strap, carrying weights, makes contact at every point tangentially. The contour was calculated in such a way that at every stage of elongation of the specimen, it compensates for the reduction in the area of cross-section of the specimen so that the stress acting on it remained constant. The creep elongation was measured using a LVDT transducer with an amplifier and recorder. With the recorder chart driven by a synchronous motor at a known constant speed, the time-extension curves during creep were recorded on the chart. The accuracy of the strain measurement was 1×10^{-5}. An extensometer was also designed to enable the measurement of creep strain on the gauge length of the sample. Testing at low temperatures was carried out by surrounding the sample, fixed in a cage shown, with appropriate cryogenic liquids. The creep testing procedure was as follows: The sample, kept at the required temperature, was loaded initially in steps of about 1 kg/mm^2 until creep was observed on the recorder chart. Creep curves were recorded at stress intervals of about 0.5 kg/mm^2. When appreciable creep rate was noticed, a small incremental load was added and the incremental creep curve recorded for some time. The incremental load was then removed to get the decremental creep curve. When this creep rate reached a low value, incremental load was again added and the process of stress addition and removal repeated till the creep rate became too low to be recorded accurately. A major stress of about 0.5 kg/mm^2 was then added and the procedure repeated.

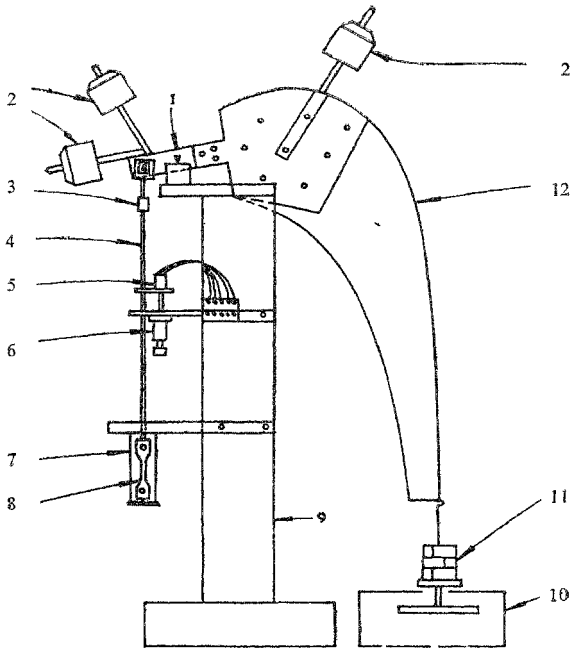

FIG. 3

Schematic sketch of the constant stress creep testing unit:
(1) Lever beam (2) compensating weights (3) ball joint (4) stainless steel pull rod (5) LVDT transducer (6) micrometer (7) specimen cage (8) specimen (9) I-beam support (10) oil dash pot (11) weights (12) contour.

Temperatures other than atmospheric range were achieved using suitable liquid baths. The baths which were not at constant boiling temperatures were stirred to achieve uniform temperature. Table I shows how the test temperatures were obtained.

TABLE 1

Temperature, °K	Medium	Temperature measurement
86	Liquid oxygen	Cu-constantan Thermocouple
195	Dry ice + alcohol	do
300	Room temperature	Mercury thermometer
373	Thermostatically heated paraffin oil	do
473	do	do

4. RESULTS

Tensile tests. Figs. 4 and 5 give the true stress-true strain curves at different temperatures indicated in the graph at a constant strain rate of 1.8×10^{-4} and 7.8×10^{-4} per second respectively. The importance of the influence of temperature on the strain hardening is evident. Fig. 4 is replotted with the true stress, σ and true strain ϵ, on a logarithmic scale and is shown in Fig. 6. Only over a limited range of strain, the approximate relation,

$$\sigma = k\,\epsilon^m$$

is obeyed. The strain hardening exponent, m, is calculated from the slope of the log-log plots at a strain value of 0.2 for the data at the strain rate of 1.8×10^{-4} per second and is plotted as a function of temperature in Fig. 7. It can be seen that the temperature influences the strain hardening coefficient significantly. The percentage elongation to fracture and to ultimate tensile stress (UTS) is also plotted in Fig. 8 as a function of temperature. There is a significant increase in percentage elongation in the low temperature range and this falls off with increase in temperature in agreement with the earlier observations[21] on pure *f.c.c.* metals.

The temperature variation of the flow stress, taken as proof stress at different strain off-set values is given in Fig. 9. It is to be noted that the temperature dependence of flow stress in the commercial metal is much more than in pure aluminum.[10] The values of ultimate tensile stress are also plotted in Fig. 10 as a function of temperature to elucidate the significant dependence of work hardening on temperature in the commercial metal compared with pure aluminum.

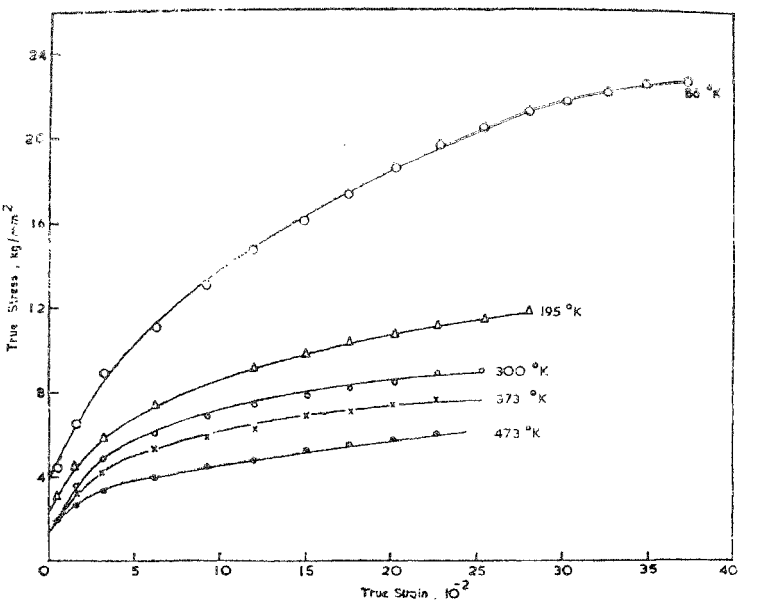

FIG. 4

True stress–true strain curves for commercial aluminum tested at a strain rate of 1.8×10^{-4} sec^{-1}.

Creep data. The nature of the creep was found[1] to be logarithmic at and below room temperature. The typical nature of the creep curve during change-in-stress creep experiments at 86°K is shown in Fig. 11. To get the magnitude of the change in creep rate following increments and also decrements, the data are replotted as true creep strain versus logarithm of time in Fig. 12. The slope (α) of each linear portion of the curve is used to calculate the creep rate $\dot{\epsilon}$ at different values of creep strain ϵ (defined at each value of time t) since $\dot{\epsilon} = \alpha/t$. The calculated creep rate is plotted on a log scale as a function of creep strain ϵ as shown in Fig. 13. This gives directly $\Delta \ln \dot{\epsilon}$ at the strain where increment/decrement is made, for the calculation of the flow parameter B from Eqn. [4]. For the purpose of this calculation, applied stress σ is converted into shear stress τ by assuming $\tau = \sigma/2$.

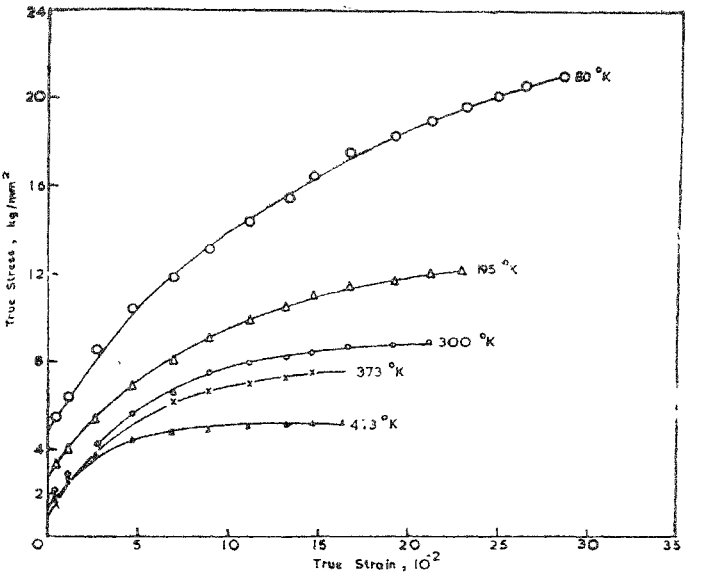

FIG 5

True stress—true strain curves for commercial aluminum tested at a strain rate of 7.8×10^{-4} sec^{-1}.

5. DISCUSSION

The results clearly show that the temperature of testing affects significantly the nature of the strain hardening in commercial aluminum compared with pure aluminum. The data on the change-in-stress creep experiments and the temperature dependence of flow stress would be very helpful in arriving at some details regarding the mechanism of strain hardening in the commercial aluminum. The following gives an analysis of the results which are aimed at evaluating activation volume and total activation energy in commercial aluminum.

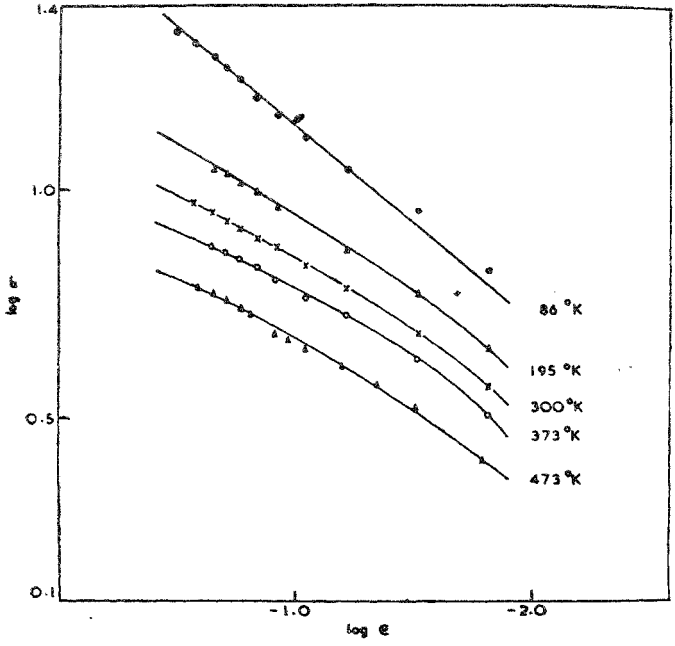

FIG. 6

Log true stress versus log true strain plots for the curves given in Fig. 4.

Substitution of Eqn. 5 in Eqn. 2 gives the temperature dependence of flow stress :

$$\tau = \tau_G + (U_0/v) - (kT/v)\ ln\ (NAbv/\dot{\varepsilon}) \qquad \text{for } T < T_c$$

and $$\tau = \tau_G \qquad \text{for } T > T_c$$

where T_c, the temperature above which the flow stress is temperature independent, is given by :

$$U_0 = kT_c\ ln\ (NAbv/\dot{\varepsilon}) \qquad [7]$$

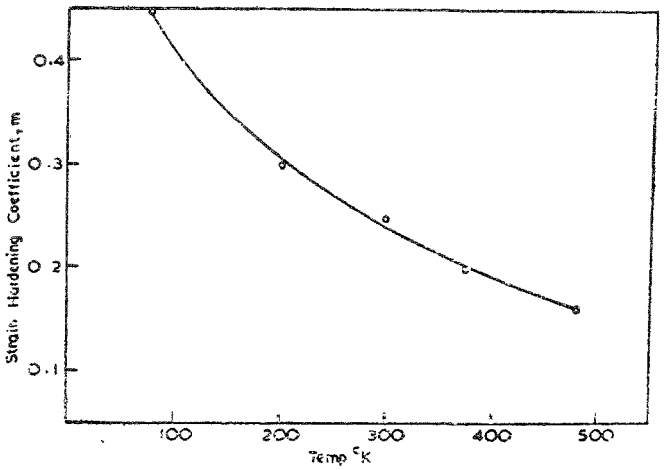

FIG. 7

Variation of strain hardening exponent m taken at a strain of 0.2 for tests at 1.8×10^{-4} sec^{-1} strain rate.

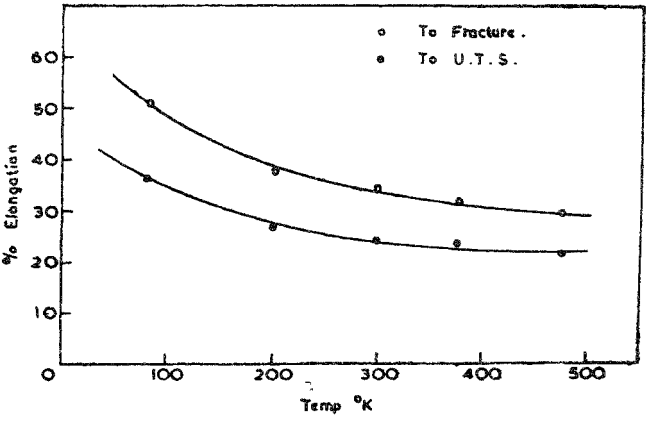

FIG. 8

Plot showing the variation of percentage elongation with temperature.

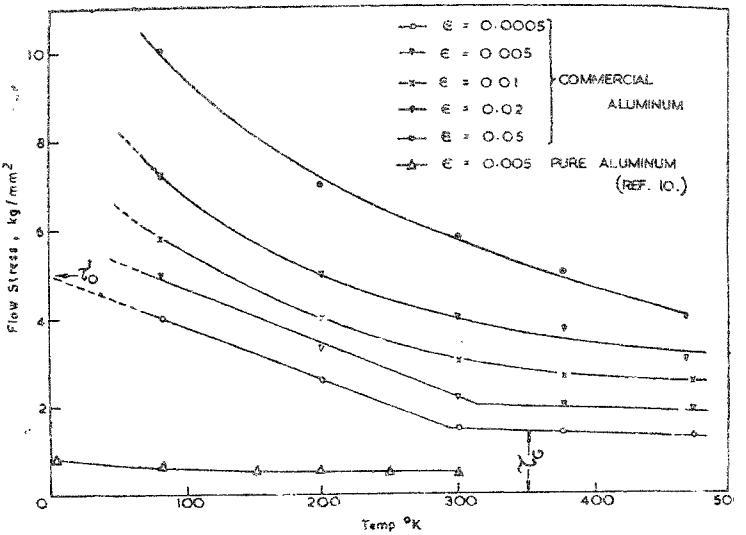

FIG 9

Plot showing the dependence of flow stress taken at different strain off-set values, as a function of temperature of testing at the strain rate of 1.8×10^{-4} per second.

From Fig. 9 the value of T_c appears to be about room temperature. The activation volume obtained from change-in-stress creep experiments is approximately 2×10^{-21} cm^3, and agrees well with that ($10^2b^3 - 10^4b^3$) to be expected for the intersection mechanism[22]. The product of v and τ is plotted as a function of strain in Fig. 14 and is found approximately constant in the stress range studied (Cottreli-Stokes law). An average value of $v\tau = 1.7\times10^{-18}$ kg-cm is taken for further calculations.

An approximate estimate of the value of U_0 could be obtained by following the method of Thornton and Hirsch[7]. The method assumes Seeger's theory of temperature dependence of flow stress which is now realised to be only an approximation; hence the calculated value of U_0 will have to be used with some caution. However, it may help us to examine the nature of the mechanism of deformation. According to Seeger's theory of temperature dependence of flow stress, it is shown[12] that

$$(\tau_0/\tau_G) \simeq 1 + (U_0/v\tau)\cdot\tau_0/\tau_G \qquad [8]$$

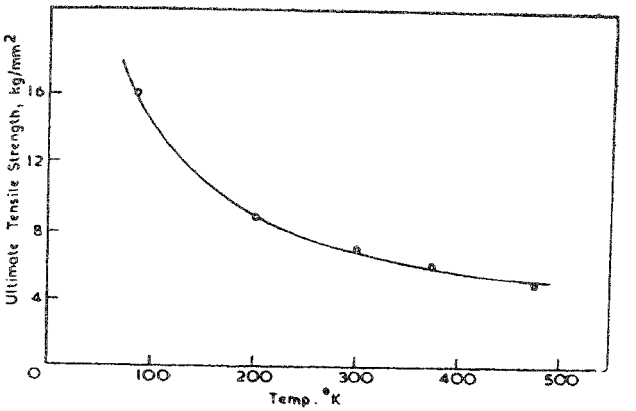

FIG. 10

Plot showing the dependence of ultimate tensile strength on temperature.

where τ_0 is the extrapolated value of flow stress at absolute zero and τ_G is the athermal part of the flow stress. From Fig. 9, (τ_0 / τ_G) is found to be $\simeq 4$, a value much higher than that reported[10] for pure aluminum ($\simeq 1{\cdot}3$). The value of U_0 calculated using the present data on the temperature dependence of flow stress is $\simeq 0.75$ *eV*. This is much higher than the theoretical jog energy value (0.1 *eV*) in aluminum[23]. It is also unlikely that the impurities present in commercial aluminum widen the stacking faults to such an extent as to increase the constriction energy (the difference between U_0 and jog energy) to 0.65 *eV*. Thus, while the estimated apparent activation volume is in agreement with that for the model of intersection of dislocations, the calculated total energy for activation appears to be different in the commercial metal than in the pure metal. This makes us think that the mechanism of intersection might not be the rate controlling mechanism in the commercial aluminum unlike in pure metal. The higher value of the estimated U_0 appears to be in accordance with the increased T_c value as is given by Eqn. 7.

Thus the observation of logarithmic creep even at room temperature, in contrast to pure aluminum which shows recovery creep[2], may be due to impurities affecting the rate-controlling mechanism in commercial aluminum. Since the observed result on U_0 does not satisfactorily confirm the intersection mechanism in commercial aluminum, one has to examine other possibilities in the light of the present data.

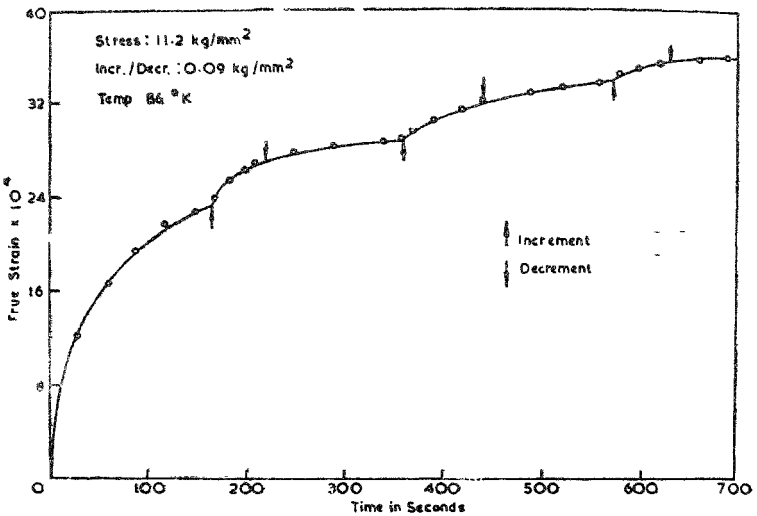

FIG. 11

Change—in—stress creep curve for commercial aluminum tested at 86°K

An alternate mechanism which can give the order of the estimated activation volume is the non-conservative motion of jogs[22]. The production of point defects by non-conservative motion of jogs in a screw dislocation can be thermally activated[24]. In a pure metal, the probability with which the dislocation jumps forward is equal to the probability of a vacancy being formed at the jog by thermal activation which is proportional to

$$\exp\left[-(E_f^v - \tau^* x L.b)/kT\right] \qquad [9]$$

where E_f^v is the vacancy formation energy.

But as the vacancy is still in the next atom position to the jog, the dislocation can jump backwards, removing the vacancy and the frequency of this movement is proportional to

$$\exp\left[+(E_f^v - \tau^* x L.b.)/kT\right] \qquad [10]$$

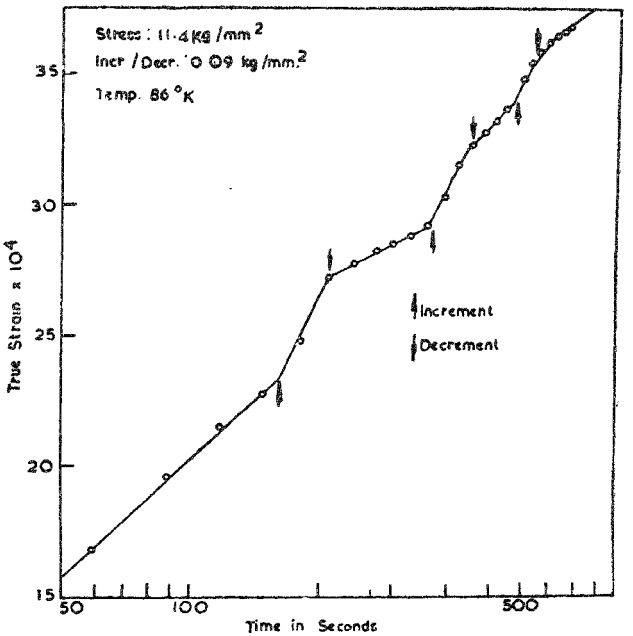

FIG. 12

Plot showing creep strain versus log time for the graph shown in Fig. 11.

Thus unless the stress term $\tau^* x$ Lb is equal to E_f^v, there will not be any net movement of the dislocation line forward[25]. Consequently the stress is virtually insensitive to temperature under these conditions. However, if the jog can move sideways and is immediately separated from the vacancy, or if the vacancy can diffuse away which requires a temperature high enough for self diffusion, the restoring force implied by expression [10] disappears and only the temperature sensitive force implied by expression [9] remains.

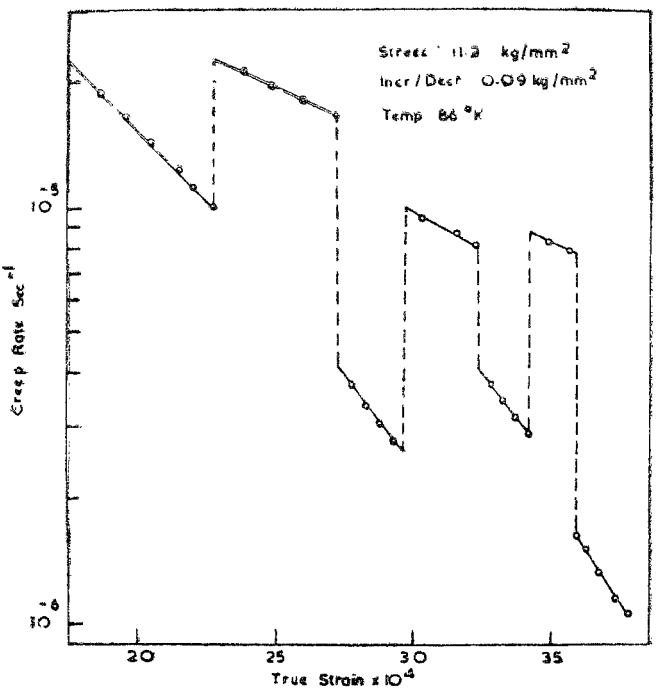

FIG. 13

Plot showing the variation of log creep rate as a function of creep strain for the curve shown in Fig. 12.

There is another possibility that has to be considered in a commercial metal. In this case the vacancy that is formed at the jog gets bound to the solute atom near the dislocation, thereby decreasing the probability of the dislocation jumping backwards given by expression [10] to

$$\exp\{+|(E_f' - E_b) - \tau^* x L\, b\,|/kT\}$$

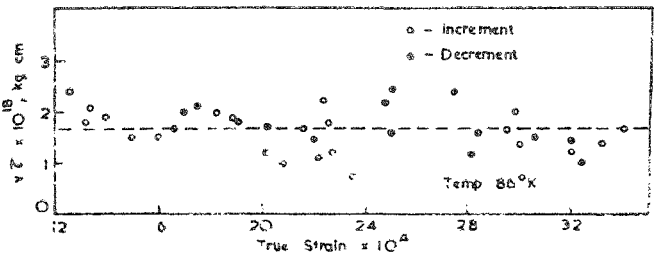

FIG. 14

Plot showing the constancy of $\nu\tau$ with strain.

where E_b = binding energy between solute atom and the vacancy. Therefore the dislocation line can make some successful forward jumps producing point defects (vacancies), the probability of which will now be given by

$$\exp\left\{-[(E_f^v - E_b) - \tau^* x L.b.]/kT\right\}$$

Depending on this model of thermally activated non-conservative movement of jogs producing vacancies which are bound to solute atoms present in the lattice, the strain rate is given by

$$\dot{\varepsilon} = NAbv \exp\left\{-[(E_f^v - E_b) - \tau^* x L.b.]/kT\right\}$$

This expression is similar to Eqn. 2 with $U_0 = (E_f^v - E_b)$. The observed value of U_0 is comparable with the apparent formation energy of vacancies in commercial aluminum which will be about 0.7 eV considering the binding energy effects between iron and silicon atoms and vacancies.

6. CONCLUSIONS

The following can be derived from the present investigations:

1. The tensile testing at low temperatures on Indian commercial aluminum showed that lowering temperature below room temperature affects significantly the nature of strain hardening compared with a pure metal.

2. The value of the total activation energy estimated from a combination of data on change-in-stress-creep experiments and temperature dependence of flow stress is about 0.75 eV, which is much higher than the value expected if intersection of dislocations were the rate controlling mechanism.

3. The observed results appear to be better explained on the basis of the model of non-conservative motion of jogs producing vacancies as the rate-controlling mechanism for thermal activation.

7. ACKNOWLEDGEMENTS

The authors are thankful to Dr. S. Dhawan, Director, Indian Institute of Science, and Professor A. A. Krishnan for their interest in this work and to other members of the Materials Research Group for their cooperation.

8. REFERENCES

1. Prasad, Y. V R. K., Sastry, D. H. and Vasu, K. I. . . *Trans. Indian Inst. Metals* (in Press)
2. Wyatt, O. H., ... *Proc. phys. Soc.*, 1953, **66**, 459.
3. Taylor, G. I., ... *Proc. R. Soc.*, 1934, **A145**, 362.
4. Nabarro, F. R. N., Basinski, Z. S. and Holt, D. B. . . *Adv. Phys.*, 1964, **13**, 193.
5. Kuhlmann-Wilsdorf, D. . . *Trans, A.I.M.E.*, 1962, **224**, 1047.
6. Mura, T. . . . . *Proc. R, Soc*, 1964, **A280**, 528; *Phil. Mag.*, 1963, **8**, 843.
7. Thornton, P. R. and Hirsch, P. B., . . *Phil. Mag*, 1958, **3**, 738.
8. Basinski, Z. S. . . . *Ibid*, 1959, **4**, 393.
9. Mitra, S. K., Osborne, P. W. and Dorn, J. E. . . *Trans. A.I.M.E.*, 1961, **221**, 1206.
10. Nunes, A. C., Rosen, A. and Dorn, J E. . . *Trans. Am. Soc. Medals*, 1965, **58**, 38
11. Mitra, S. K. and Dorn, J.E, . . *Trans. A.I.M.E.*, 1963, **227**, 1015.
12. Seeger, A. . . . . Dislocations and Mechanical Properties of Crystals, 1957, John Wiley, New York, 243.
13. Hirsch, P. B. . . . . Symposium on Internal Stresses and Fatigue in Metals, 1958, Elsevier Amsterdam, 139.
14. Cottrell, A. H and Stokes, R. J. . . *Proc. R. Soc*, 1955, **A233**, 17.
15. Lytton, J. L., Shepard, L. A. and Dorn, J. E. . . *Trans. A.I.M.E.*, 1958, **212**, 220.
16. Rocher, Y. A., Shepard, L.A. and Dorn, J. E. . . *Trans. A.I.M.E.* 1959, **215**, 316.
17. Rosen, A. and Bodner, S. R. . . *J. Mech. Phys. Solids*, 1967, **15**, 47.
18. Rosen, A. . . . . *Mat. Sci. Engg*, 1967, **2**, 117.
19. Suzuki, H. . . . . Dislocations and Mechanical Properties of Crystals, 1957, John Wiley, New York, 361.
20. Byrne, J.G., Fine, M.E. and Kelly, A. *Phil. Mag.*, 1961, **6**, 1119,
21. Carreker, R. P. and Hibbard, W.R. *Acta metall.*, 1953, **1**, 654.
22. Conrad, H. . . . . . *J. Metals*, 1964, **16**, 582.
23. Friedel, J. . . . . Dislocations, Pergamon Press, 1964, 309.
24 Hirth, J. P. and Lothe, J. . . Theory of Dislocations, 1968, McGraw-Hill Book Co. New York, 535.
25. Mott, N F. . . . . *Phil. Mag.*, 1952, **43**, 1151.